Conference paper

Yuta Saito, Paul Fons, Kirill V. Mitrofanov, Kotaro Makino, Junji Tominaga, John Robertson and Alexander V. Kolobov*

Chalcogenide van der Waals superlattices: a case example of interfacial phase-change memory

https://doi.org/10.1515/pac-2019-0105

Abstract: 2D van der Waals chalcogenides such as topological insulators and transition-metal dichalcogenides and their heterostructures are now at the forefront of semiconductor research. In this paper, we discuss the fundamental features and advantages of van der Waals bonded superlattices over conventional superlattices made of 3D materials and describe in more detail one practical example, namely, interfacial phase change memory based on GeTe–Sb_2Te_3 superlattice structures.

Keywords: GeTe; non-volatile memory; phase change materials; Sb_2Te_3; SSC-2018; structural analysis; superlattice.

Introduction

The success of graphene triggered an intensive search for other 2D materials, among which chalcogenides occupy a very special place. Among the most studied materials are topological insulators (TIs) such as Sb_2Te_3 and Bi_2Te_3 [1] and two-dimensional transition metal dichalcogenides (TMDCs) with the generic formula MX_2, where M=Mo, W and X=S, Se and Te [2]. These materials are constructed of covalently bonded blocks held together by weak van der Waals (vdW) interactions. Their structures are illustrated in Fig. 1. Recently, great efforts have been dedicated to building heterostructures and superlattices from vdW bonded materials [3]. This interest is due to several fundamental advantages offered by the 2D nature of such materials as will be discussed below.

Traditional semiconductor heterostructures and superlattices formed from 3D materials such as Si, Ge, GaAs, etc. are usually grown using epitaxy. Epitaxial growth techniques, such as molecular beam epitaxy (MBE), allow fabrication of semiconductor structures with atomic layer precision, but possess

Article note: A collection of invited papers based on presentations at The 13th International Conference on Solid State Chemistry (SSC-2018), Pardubice, Czech Republic, September 16–21, 2018.

***Corresponding author: Alexander V. Kolobov,** National Institute of Advanced Industrial Science and Technology, Tsukuba, Japan; and Herzen State Pedagogical University, Faculty of Physics, St. Petersburg, Russian Federation, e-mail: a.kolobov@herzen.spb.ru. https://orcid.org/0000-0002-8125-1172

Yuta Saito: Nanoelectronics Research Institute, National Institute of Advanced Industrial Science and Technology, Tsukuba, Japan; and Department of Engineering, University of Cambridge, Cambridge, United Kingdom of Great Britain and Northern Ireland. https://orcid.org/0000-0002-9576-1560

Paul Fons, Kirill V. Mitrofanov, Kotaro Makino and Junji Tominaga: Nanoelectronics Research Institute, National Institute of Advanced Industrial Science and Technology, Tsukuba, Japan. https://orcid.org/0000-0002-7820-1924 (P. Fons); https://orcid.org/0000-0002-2775-4123 (K. V. Mitrofanov); https://orcid.org/0000-0002-2122-1617 (K. Makino); https://orcid.org/0000-0002-6433-6916 (J. Tominaga)

John Robertson: Department of Engineering, University of Cambridge, Cambridge, United Kingdom of Great Britain and Northern Ireland

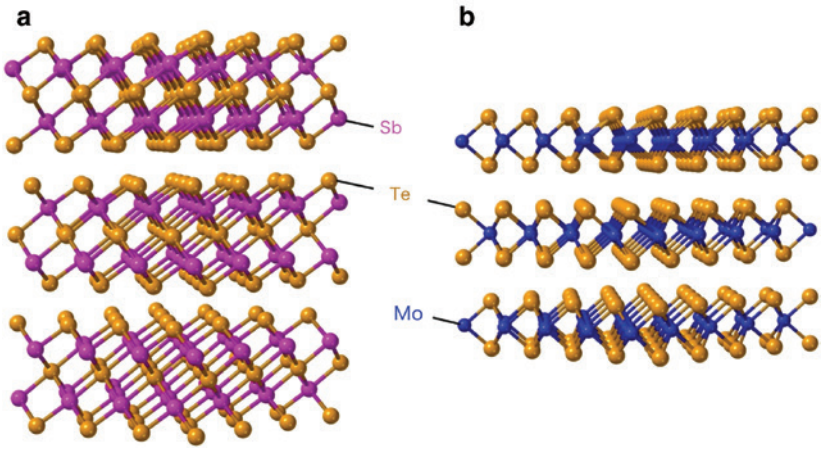

Fig. 1: Crystal structures of representative 2D chalcogenides (a) Sb_2Te_3 (TI) and (b) $MoTe_2$ (TMDC).

some caveats. In particular, the substrate and the overlayer must have similar lattice constants and symmetry as well as thermal behavior, which significantly limits the possible combinations. If the lattice constant of the substrate and the overlayer differ, the strain in the overlayer can change the growth process from a layer-by-layer mode to the Stranski–Krastanov mode, where islands, rather than a continuous layer, are formed (Fig. 2a) [4]. In addition, strain can drive interdiffusion as is illustrated in Fig. 2b,c for the case of Ge grown on Si. In Fig. 2b we show the Ge K-edge X-ray absorption near-edge structure (XANES) spectra of bulk Ge and of a thin Ge layer grown (non-epitaxially) on oxidized silicon. XANES is a powerful structural tool to analyze local structure. We do not go into details of XANES theory and measurement here but use XANES spectra as a fingerprint of a structure. As can be seen, the two spectra shown in Fig. 2b are essentially identical demonstrating the formation of a phase similar to that of bulk Ge. In contrast, the Ge K-edge XANES spectrum of a thin Ge layer epitaxially grown on Si and subsequently capped by silicon is indistinguishable from that of a dilute solid solution of Ge in Si, indicating very strong intermixing, where an alloy instead of a Si–Ge–Si heterostructure, is formed (Fig. 2c) [6]. To conclude this section, two essential problems occur during conventional epitaxy when the lattice parameters of a heterostructure do not match, namely (i) the overlayer can grow as 3D islands rather than a continuous 2D layer and (ii) strong intermixing can occur.

On the other hand, the use of atomically flat surfaces of 2D materials, which do not contain any dangling bonds, and hence no covalent bonds between the substrate and overlayer are formed, theoretically offer the

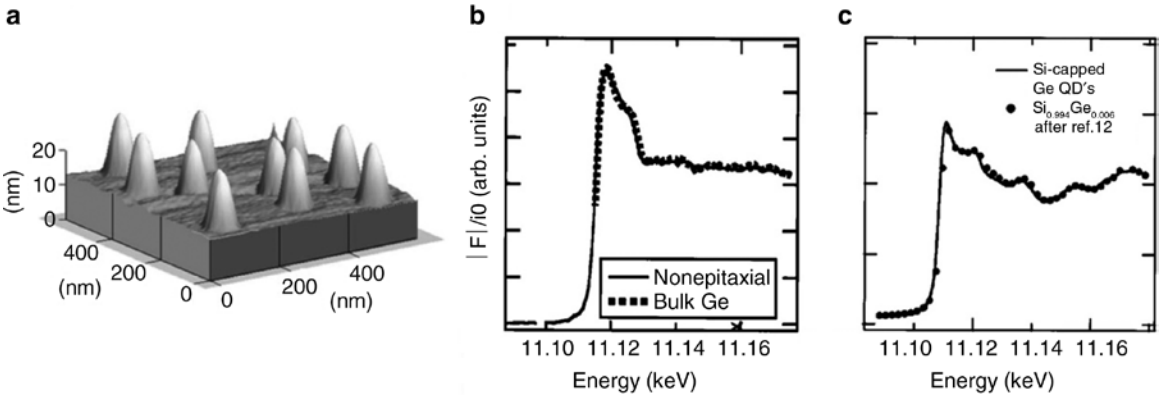

Fig. 2: (a) Ge quantum dots grown on Si(001) via the Stranski–Krastanov growth mode [4]. A comparison of the XANES spectra of (b) non-epitaxial [5] and (c) epitaxial Ge grown on silicon with bulk Ge and $Si_{0.994}Ge_{0.006}$ references [6]. Panel (a) is reproduced with permission from Elsevier, panels (b,c) are reproduced with permission from AIP Publishing.

possibility of combining materials with atomically sharp interfaces even in the presence of significant lattice mismatch. This technique, known as van der Waals epitaxy was first proposed in the 1980s [7, 8] and recently has attracted renewed attention for the growth of both 2D and also for conventional 3D materials, such as GaN grown on graphene [9].

In what follows we shall focus on GeTe/Sb_2Te_3 superlattices, also known as interfacial phase-change memory, as an example of an interesting application focused chalcogenide superlattice. The development of phase-change materials for memories, where the information is stored as structural states (amorphous vs. crystalline), dates back over three decades [10, 11], with the most studied materials being Ge–Sb–Te ternary alloys on the GeTe–Sb_2Te_3 pseudobinary tie-line. They have been successfully used to fabricate re-writable optical discs, from compact discs to Blu-ray [12], and are also one of the most promising candidates for the next generation non-volatile memory. In particular, 3D XPoint memory technology, where the three-dimensional integration of chalcogenide-based memory and selector components enables much denser capacity than dynamic random access memory (DRAM) and faster writing speeds than Flash, was recently commercialized by Intel and Micron [11].

The recently proposed interfacial phase change memory (iPCM), where GeTe and Sb_2Te_3 are spatially separated in form of an atomically aligned superlattice with vdW gaps separating covalently bonded blocks is characterized by significantly faster switching, lower energy consumption and better endurance [13–16]. It is interesting to note that despite the rather simple preparation method used (sputtering), a layered structure with well-defined vdW gaps was obtained when an Sb_2Te_3 seed layer was pre-deposited prior to the GeTe deposition [17, 18], clearly demonstrating the important role of a 2D material in promoting the layered overgrowth of a 3D material. Intermixing was not studied in the initial work and will be discussed in detail below.

After the initial demonstration of the superior performance of iPCM, models based on the rearrangement of Ge and Te planes within GeTe blocks were proposed as illustrated in Fig. 3. In particular, first-principles simulations showed that while the Kooi phase (see Fig. 3 for notations) has the lowest energy at low temperatures, at elevated temperatures the ferro phase where the stacking order of the GeTe block is similar to that of bulk GeTe becomes energetically favorable. Based on these results, a transition between different phases within GeTe blocks was suggested to be at the origin of iPCM switching [19–22].

Subsequent TEM investigation of epitaxially grown samples revealed that isolated GeTe blocks do not exist in GeTe/Sb_2Te_3 superlattices but instead Ge atoms are located inside the covalent blocks with Sb atoms forming the cation plane closest to the vdW gap [23–25]. While it should be kept in mind that the TEM results refer to samples grown in thermal equilibrium, which do not necessarily correspond to the SET and/or RESET states obtained through application of short pulses and thus are kinetically limited, they nevertheless called for a reconsideration of the earlier models. It was initially argued that GeTe blocks dissolve within Sb_2Te_3 thanks to interdiffusion of Ge and Sb during the growth process [26] but later an alternative explanation was offered in terms of initial termination of the 3D surface of GeTe by an SbTe bilayer, which changes the growth sequence for the GeTe/Sb_2Te_3 SL to the Kooi-like phase [27]. It is also interesting to note that despite the use of a very precise technique such as MBE, the local structure of the grown samples differs from the global

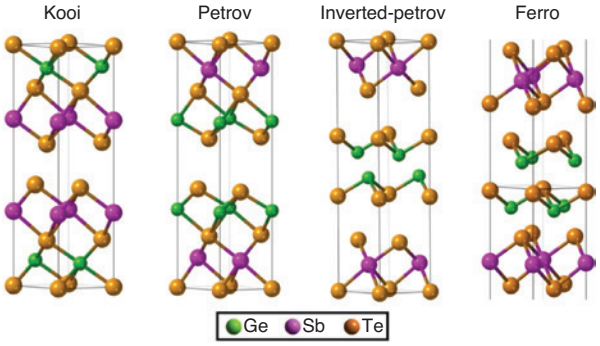

Fig. 3: Originally proposed structural models for the GeTe/Sb_2Te_3 superlattice [21].

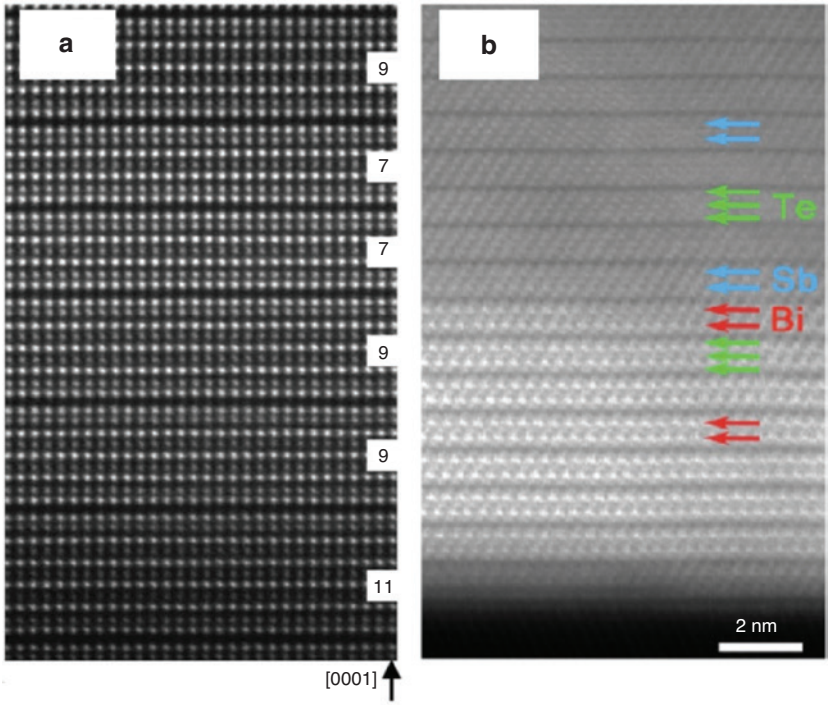

Fig. 4: Numerous stacking faults in a (a) Ge–Sb–Te superlattice [30] as opposed to a perfect array of quintuple layers in a (b) Bi_2Te_3–Sb_2Te_3 heterostructure [31]. Panel (a) is adapted from the original work published by Macmillan Publishers Limited under a Creative Commons Attribution 4.0 International License. Panel (b) is reproduced with permission from American Chemical Society.

structure. In particular, while the average composition was $Ge_2Sb_2Te_5$ where nine-layer covalent blocks were expected, the experimental sample was a mixture of odd-layer (5, 7, 9, 11, etc.) blocks suggesting that terminating bilayers can easily switch across vdW gaps. This process, called dynamical vdW gap reconfiguration, was observed by several groups and is illustrated in Fig. 4a seems to be an inherent feature of iPCM [28, 29]. At the same time, a similar gap reconfiguration is not observed in the Sb_2Te_3 end composition or in Bi_2Te_3–Sb_2Te_3 heterostructures, where perfect arrays of quintuple layers were formed (Fig. 4b), suggesting a crucial role for Ge atoms in initiating the bilayer crossover switching process. Below, we discuss our recent results on the local structure of Ge atoms in iPCM and their mobility within the superlattice.

Experimental

Fabrication of samples

The GeTe/Sb_2Te_3 superlattices were fabricated by radio-frequency (RF) magnetron helicon sputtering (MPS or QAM-4, ULVAC Corp.) [18, 32, 33]. The films were grown on Si(001) single crystal substrates. Ge–Te and Sb–Te alloy targets were used. The thickness of each layer was controlled by the opening time of the shutter above each sputtering cathode. The growth or post-annealing temperatures were varied from room temperature to 230 °C depending on the experiment. The native oxide of the Si substrate was removed before growth by Ar reverse sputtering.

X-ray absorption spectroscopy (XAS)

XANES measurements for the Ge K-edge were carried out at room temperature in fluorescence mode at beamline BL01B1 at SPring-8 (synchrotron); the details are described in Ref. [34]. The XANES spectra were

calculated using the *ab initio* real-space full multiple-scattering code FEFF8; the details are described in Ref. [35, 36].

Secondary ion mass spectroscopy (SIMS)

SIMS samples were prepared at different growth temperatures (A: RT, B: 150 °C, C: 190 °C, and E: 230 °C), or using room temperature growth followed by post-annealing (D: 190 °C annealing and F: 230 °C annealing). The total time for the high-temperature growth process was about 10 min, while the post-annealing was carried out over 30 min. The SIMS measurements were performed using an IMS-7f, CAMECA at Tohoku University. Positively charged oxygen was used as the primary ion beam and the beam energy was set to 2.0 keV.

Transmission electron microscopy (TEM)

TEM specimens were prepared by mechanical polishing, followed by Ar-ion beam milling (Dual Mill 600, Gatan, Inc.). The cross-sectional microstructures were observed by STEM (JEM-ARM200F, JEOL Co. Ltd). The acceleration voltage was 200 kV. The probe size was 2 Å, and the probe current was 60 pA. The total acquisition time for energy-dispersive X-ray (EDX) spectroscopy mapping was about 20 min, with a dwell time of 15 µs per point.

Results and discussion

First we notice that while the simplest ideal structures are formed of pure Ge and Sb atomic planes, intercalating Te planes, in realistic samples the cations are likely to intermix. Ge/Sb intermixing was originally proposed for the hexagonal phase of $Ge_2Sb_2Te_5$ [37] and later, based on TEM and extended X-ray absorption fine structure (EXAFS) measurements it was also argued that Ge and Sb are intermixed in iPCM [23, 24]. To look more deeply into this issue, we performed a careful analysis of experimental XANES spectra using systematic simulations. XANES analysis offers an advantage over EXAFS in that the XANES features are less effected by noise than EXAFS oscillations, a factor that can be important for very thin samples and/or when it is necessary to detect minor structural differences in samples.

In Fig. 5 we compare experimental XANES spectra for two kinds of samples, namely, those with fixed thickness of one of the components and varying thickness of the other. One can see that there is no systematic trend accompanying the variation in the GeTe or Sb_2Te_3 thicknesses suggesting that these samples may possess similar local structure around the Ge species. This result is not totally unexpected considering the fact that Ge and Sb are likely to intermix. In particular, we note that all spectra contain a peak located 10 eV above the white line (the first strong peak in the spectra).

Figure 6 shows the experimental XANES spectrum of a [GeTe (1 nm)/Sb_2Te_3 (1 nm)] 20 superlattice film together with the simulated XANES spectra of the original four models. One can see that none of these models reproduces the experimental spectrum (Fig. 6a), strongly suggesting that the real superlattice structure is more complicated than the simplistic earlier models. As two or more model structures may co-exist, additional fitting of the experimental spectra by a weighted combination of the four models based upon a genetic fitting algorithm was carried out (Fig. 6b). However, even the best fit with approximate weights 2/5IP + 2/5P + 1/5K (the abbreviations originate from the first letters of each model as shown in Fig. 3) could not reproduce the shoulder peak at around 10 eV above the white line in the experimental data, shown by the black arrow.

We then extended the range of structure models used as input to the XANES simulations in order to investigate the effect of Ge and Sb intermixing, Fig. 7a compares two different models for the $Ge_3Sb_2Te_6$ (GST326) composition. The non-mixed phase GST326 based the Kooi model has the atomic stacking ⋯ Te–Sb–Te–Ge–Te–Ge–Te–Ge–Te–Sb–Te ⋯ (where – and ⋯ represent covalent bonding and vdW bonding, respectively).

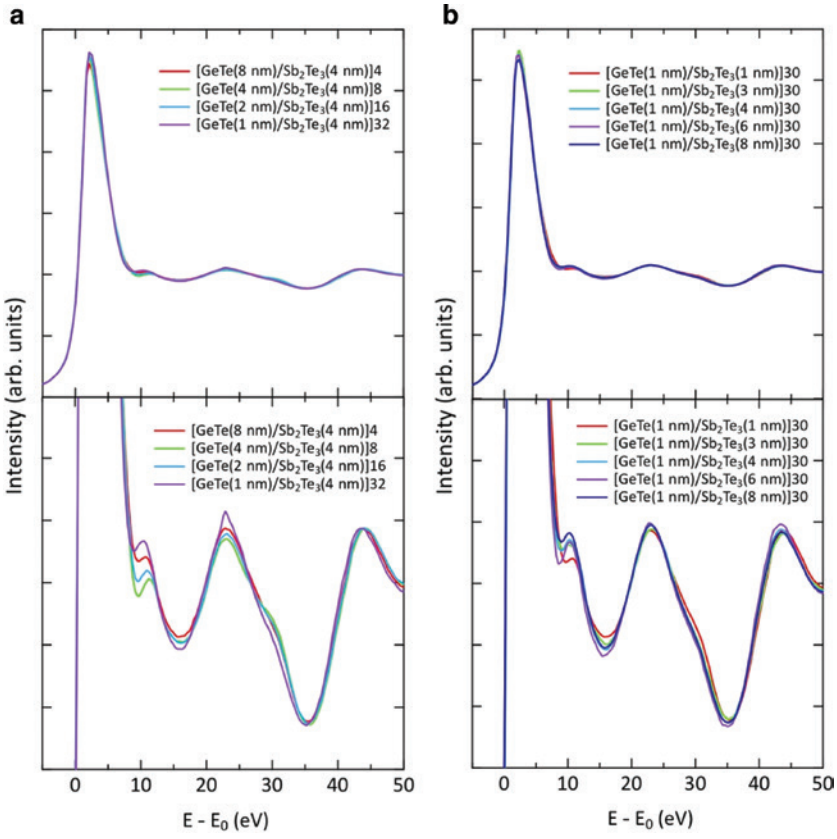

Fig. 5: XANES spectra for superlattice films with different block thicknesses. (a) is GeTe (x nm)/Sb_2Te_3 (4 nm) (x = 1–8 nm) and, (b) is GeTe (1 nm)/Sb_2Te_3 (y nm) (y = 1–8 nm). Bottom panels are zoom-ins along the vertical axis.

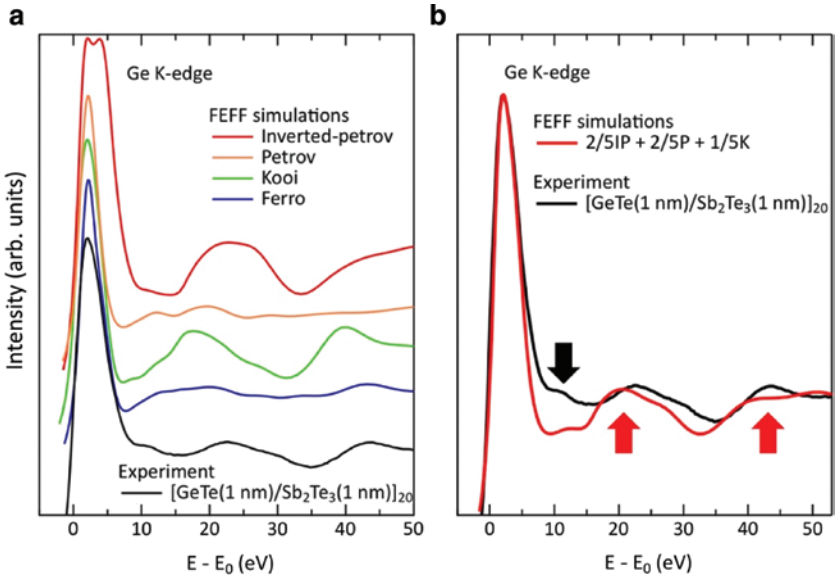

Fig. 6: (a) Experimental XANES spectrum of [GeTe (1 nm)/Sb_2Te_3 (1 nm)]$_{20}$ superlattice film together with simulated XANES spectra of the original four models. (b) Fitting of experimental XANES spectrum by three different models with optimal weighting.

The key feature of this structure is that only Sb atomic layers are located next to the vdW gap, with Ge atoms lying at the center of vdW blocks. In an alternative model $\cdots$ Te–$Ge_{50}Sb_{50}$–Te–$Ge_{50}Sb_{50}$–Te–Ge–Te–$Ge_{50}Sb_{50}$–Te–$Ge_{50}Sb_{50}$–Te $\cdots$ shown in Fig. 7a, Sb and Ge species are intermixed.

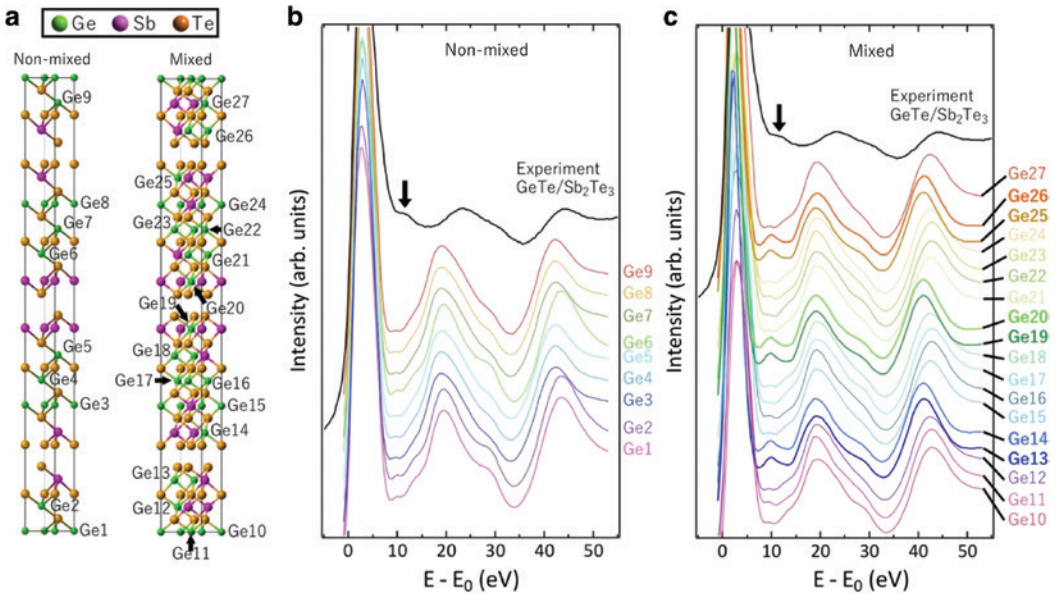

Fig. 7: (a) Structure models of GST326 where the non-mixed structure represents the ··· Te–Sb–Te–Ge–Te–Ge–Te–Ge–Te–Sb–Te··· stacking sequence by analogy to the Kooi stacking sequence. The mixed model includes Ge/Sb intermixing. Simulated XANES spectra as well as the experimental result for (b) non-mixed and (c) mixed models. Simulations were carried out for all individual Ge atoms.

XANES simulations were carried out for these two models and the results are shown in Fig. 7b, c together with the experimental spectrum. All Ge atoms in the non-mixed model show similar spectra and the shoulder peak feature is absent. On the other hand, intriguingly, some Ge atoms in the mixed model show a pronounced peak after the main absorption peak (as indicated in the figure with a bold font and thicker lines) analogous to the shoulder observed in experiment. We found that a common feature of the Ge atoms giving rise to this feature (Ge atoms 13, 14, 19, 20, 25, and 26) was that all these atoms were located next to the vdW gap. On the other hand, this feature is absent for Ge atoms located inside the vdW blocks such as Ge12 in the mixed model. This result strongly suggests the presence of Ge atoms close to the vdW gap, which is in full agreement with the conclusions reached previously from TEM [23, 25] and EXAFS [24] studies. It should be noted that the XANES spectra of superlattices are very similar to that of the GeTe crystalline film [34]. In the previous work, some of the present authors tried to reproduce the experimental results using several GeTe models including rhombohedral and cubic structures. However, none of the models could explain the bump at 10 eV above the absorption edge. These results indicated that real GeTe thin film samples may contain defects and differ from the ideal structure model. The current work successfully demonstrates the bump feature for the first time by taking into account Ge atoms close to the vdW gaps in the $GeTe/Sb_2Te_3$ superlattice. If this is also the case for GeTe, one can assume that there are similar stacking faults in the GeTe film, namely, not the ideal alternate stacking like –Ge–Te–Ge–Te–Ge–Te–, but –Ge–Te···Te–Ge–Te–Ge–Te–. The existence of Ge atoms close to the stacking fault, i.e. vdW gaps, might result in the bump feature. Our earlier work using pair correlation analysis demonstrating that the alpha to beta GeTe transition is not displacive, but is an order-disorder transition also suggests that the structure of GeTe may be more dynamic than the usually accepted model [38]. Therefore, we believe that detailed studies of crystalline GeTe film on the atomic-scale level would be helpful in understanding the structural dynamics of superlattice films as well, and this will be a future work.

Next, we studied the global diffusivity of Ge throughout the film. To understand the diffusion dynamics, multi-layer samples (as shown in Fig. 8a) were prepared at different temperatures and SIMS depth profiling was carried out. Figure 8b shows a typical result of a SIMS depth scan. After the etching of the W cap layer was complete, both the Sb and Te signals were found to sharply increase indicating the depth profile had reached the top surface of the Sb_2Te_3 layer; this was followed by an increase in the Ge intensity. To demonstrate the effect of temperature, Ge profiles are compared in Fig. 8c. The Sb and Te profiles did not change

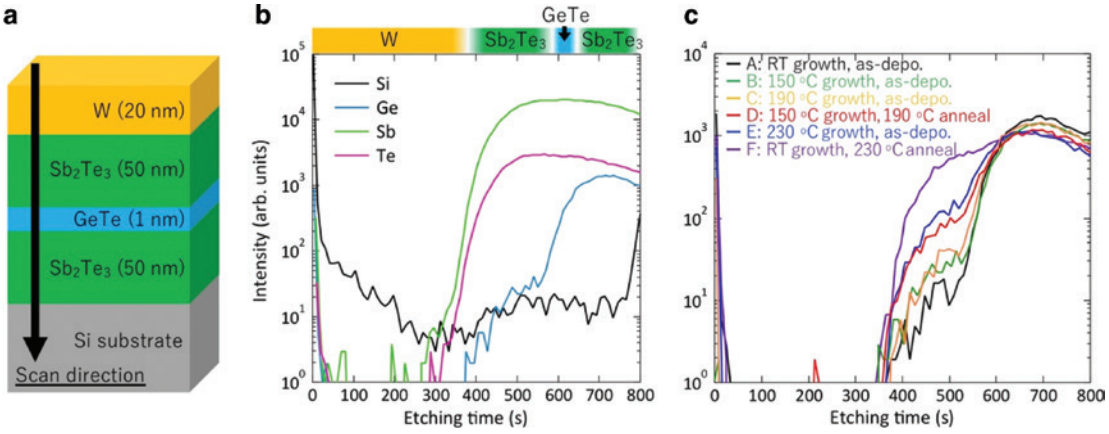

Fig. 8: (a) Schematic image of the sample structure used for SIMS analysis. (b) Depth profiles for the four elements of the sample grown at 150 °C. (c) Comparison of the Ge profiles for different samples, where the growth and/or post-annealing temperatures are shown.

and are not shown in order to better visualize the diffusion of Ge. A pronounced variation in the Ge intensity was observed demonstrating that at elevated (but still rather low) temperatures Ge atoms can easily diffuse through 50 nm of Sb_2Te_3.

Additional experimental evidence for fast Ge diffusion is presented in Fig. 9, which shows a cross-sectional high angle annular dark field (HAADF) scanning transmission electron microscopy (STEM) image of a GeTe/Sb_2Te_3 superlattice film with elemental mapping obtained by EDX spectroscopy. Sb and Te atoms were found to alternately stack as shown in the overlapped image (Sb + Te). The intensity of the Sb signal was relatively high close to the vdW gap, but interestingly it also remained non-zero inside the vdW blocks, again suggesting the existence of Sb atoms within the vdW blocks, i.e. Ge/Sb intermixing discussed above. At the same time, the elemental mapping results for Ge demonstrate that Ge atoms are not well localized but, rather delocalized. This result can be understood as being a consequence of electron-induced migration during the STEM-EDX scan, where the region was rastered over a 20-min period by a focused electron beam.

We speculate that under intense electronic excitations Ge atoms from the covalently bonded blocks are excited into vdW gaps, where they can easily move hopping from one tetrahedral vacancy to another in a process similar to alkali metal intercalation in TMDCs. We also note that the fast diffusivity of Ge atoms in

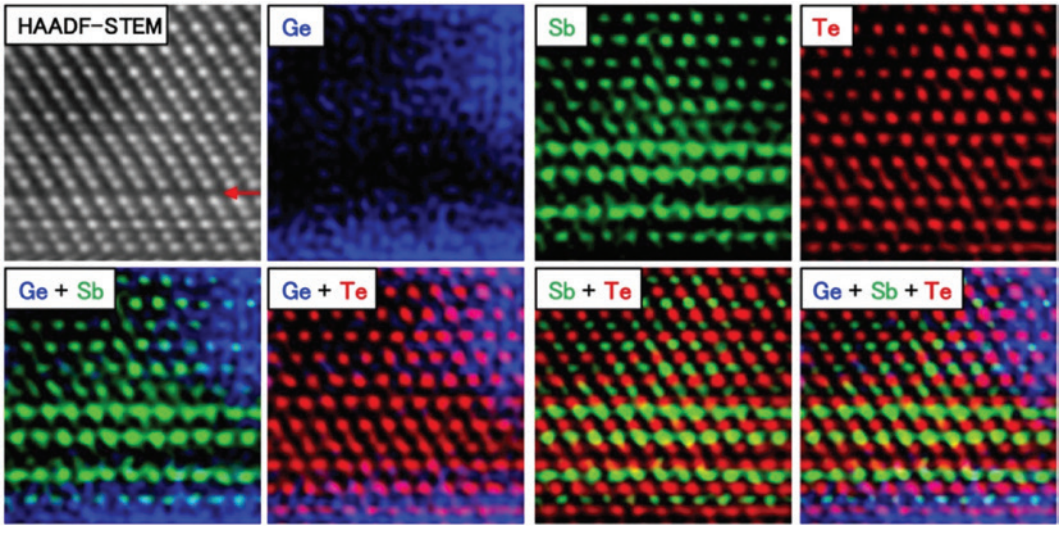

Fig. 9: HAADF-STEM images of the superlattice film with elemental mapping results obtained by EDX analysis.

GST is consistent with previously reported *ab initio* molecular dynamics simulations [39]. In particular, Wang et al. recently have reported that the fast diffusion of Ge atoms around the vdW gaps plays an important role in the *quasi*-two-dimensional amorphization process in the Ge–Sb–Te alloy, supporting our experimental findings in this work [40]. These results demonstrate significantly stronger diffusivity of the Ge species compared to Sb and Te and suggest that Ge species play a vital role in the switching process of iPCM. The details of a possible phase-change mechanism that involves both Ge atoms switching and subsequent Sb atoms diffusion leading to a pronounced resistivity contrast in iPCM have been discussed elsewhere [41].

Finally, we would like to note that while atomically sharp interfaces were reported for the epitaxial growth of TMDCs [42], in $GeTe/Sb_2Te_3$ SLs cations strongly intermix. We note here that rather strong interdiffusion was also reported for Bi_2Te_3/Sb_2Te_3 heterostructures [31], clearly indicating that obtaining diffusionless interfaces even in the case of vdW epitaxy is not straightforward.

Conclusions

In conclusion, 2D chalcogenides are an interesting playground to grow heterostructures and superlattices through vdW epitaxy, especially for cases when the substrate and overlayer are not lattice matched. However, even in this case intermixing is not completely suppressed. For the example of iPCM, we demonstrated Ge/Sb intermixing and the ability of Ge species to diffuse at large distances, especially under the effect of intense electronic excitation. We believe that the ease with which Ge atoms can migrate is a crucial feature that enables fast switching of iPCM.

Acknowledgements: This study was supported by JST CREST, Funder Id: http://dx.doi.org/10.13039/501100003382, No. JPMJCR14F1, and KAKENHI, Japan Society for the Promotion of Science, Funder Id: http://dx.doi.org/10.13039/501100001691, Nos. JP16K04896 and 18K14306. XAFS measurements were performed at beamline BL01B1 at SPring-8 as a part of Proposals No. 2012B1303 and No. 2014A1342. We thank Dr. Toshiaki Ina of SPring-8 for his assistance in XAS measurements. We also thank Dr. Takamichi Miyazaki of Tohoku University for his assistance in SIMS measurements, and Kosuke Kurushima of TORAY for his assistance in TEM observations.

References

[1] H. Zhang, C.-X. Liu, X.-L. Qi, X. Dai, Z. Fang, S.-C. Zhang. *Nat. Phys.* **5**, 438 (2009).
[2] M. Chhowalla, D. Jena, H. Zhang. *Nat. Rev. Mater.* **1**, 16052 EP (2016).
[3] A. K. Geim, I. V. Grigorieva. *Nature* **499**, 419 (2013).
[4] K. Wang, J. Liu, G. Jin. *J. Cryst. Growth* **237–239**, 1892 (2002).
[5] A. V. Kolobov, A. A. Shklyaev, H. Oyanagi, P. Fons, S. Yamasaki, M. Ichikawa. *Appl. Phys. Lett.* **78**, 2563 (2001).
[6] A. V. Kolobov, H. Oyanagi, K. Brunner, P. Schittenhelm, G. Abstreiter, K. Tanaka. *Appl. Phys. Lett.* **78**, 451 (2001).
[7] A. Koma, K. Sunouchi, T. Miyajima. *Micro. Eng.* **2**, 129 (1984).
[8] A. Koma. *Thin Solid Films* **216**, 72 (1992).
[9] T. Li, C. Liu, Z. Zhang, B. Yu, H. Dong, W. Jia, Z. Jia, C. Yu, L. Gan, B. Xu. *AIP Adv.* **8**, 045105 (2018).
[10] M. Wuttig, N. Yamada. *Nat. Mater.* **6**, 824 (2007).
[11] P. Noé, C. Vallée, F. Hippert, F. Fillot, J.-Y. Raty. *Semi. Sci. Tech.* **33**, 013002 (2018).
[12] N. Yamada, E. Ohno, K. Nishiuchi, N. Akahira, M. Takao. *J. Appl. Phys.* **69**, 2849 (1991).
[13] R. E. Simpson, P. Fons, A. V. Kolobov, T. Fukaya, M. Krbal, T. Yagi, J. Tominaga. *Nat. Nanotech.* **6**, 501 (2011).
[14] J. Tominaga. *MRS Bulletin* **43**, 347 (2018).
[15] J. Tominaga. *Phys. Stat. Sol. (RRL)* DOI:10.1002/pssr.201800539, 1800539 (2018).
[16] X.-B. Li, N.-K. Chen, X.-P. Wang, H.-B. Sun. *Adv. Funct. Mater.* **28**, 1803380 (2018).
[17] R. E. Simpson, P. Fons, A. V. Kolobov, M. Krbal, J. Tominaga. *Appl. Phys. Lett.* **100**, 021911 (2012).
[18] Y. Saito, P. Fons, A. V. Kolobov, J. Tominaga. *Phys. Stat. Sol. (B)* **252**, 2151 (2015).
[19] J. Tominaga, P. Fons, A. Kolobov, T. Shima, T. C. Chong, R. Zhao, H. K. Lee, L. Shi. *Jap. J. Appl. Phys.* **47**, 5763 (2008).

[20] T. Ohyanagi, M. Kitamura, M. Araidai, S. Kato, N. Takaura, K. Shiraishi. *Appl. Phys. Lett.* **104**, 252106 (2014).
[21] J. Tominaga, A. V. Kolobov, P. Fons, T. Nakano, S. Murakami. *Adv. Mat. Interfaces* **1**, 1300027 (2014).
[22] X. Yu, J. Robertson. *Sci. Rep.* **5**, 12612 (2015).
[23] J. Momand, R. Wang, J. E. Boschker, M. A. Verheijen, R. Calarco, B. J. Kooi. *Nanoscale* **7**, 19136 (2015).
[24] B. Casarin, A. Caretta, J. Momand, B. J. Kooi, M. A. Verheijen, V. Bragaglia, R. Calarco, M. Chukalina, X. Yu, J. Robertson, F. R. L. Lange, M. Wuttig, A. Redaelli, E. Varesi, F. Parmigiani, M. Malvestuto. *Sci. Rep.* **6**, 22353 (2016).
[25] A. Lotnyk, I. Hilmi, U. Ross, B. Rauschenbach. *Nano Res.* **11**, 1676 (2017).
[26] R. Wang, V. Bragaglia, J. E. Boschker, R. Calarco. *Cryst. Growth Des.* **16**, 3596 (2016).
[27] A. V. Kolobov, P. Fons, Y. Saito, J. Tominaga. *ACS Omega* **2**, 6223 (2017).
[28] A. Lotnyk, U. Ross, T. Dankwort, I. Hilmi, L. Kienle, B. Rauschenbach. *Acta Mater.* **141**, 92 (2017).
[29] J. Momand, R. Wang, J. E. Boschker, M. A. Verheijen, R. Calarco, B. J. Kooi. *Nanoscale* **9**, 8774 (2017).
[30] A. Lotnyk, U. Ross, S. Bernütz, E. Thelander, B. Rauschenbach. *Sci. Rep.* **6**, 26724 EP (2016).
[31] M. Lanius, J. Kampmeier, C. Weyrich, S. Kölling, M. Schall, P. Schüffelgen, E. Neumann, M. Luysberg, G. Mussler, P. M. Koenraad, T. Schäpers, D. Grützmacher. *Cryst. Growth Des.* **16**, 2057 (2016).
[32] Y. Saito, P. Fons, L. Bolotov, N. Miyata, A. V. Kolobov, J. Tominaga. *AIP Adv.* **6**, 045220 (2016).
[33] Y. Saito, K. V. Mitrofanov, K. Makino, N. Miyata, P. Fons, A. V. Kolobov, J. Tominaga. *ECS Trans.* **86**, 49 (2018).
[34] A. V. Kolobov, P. Fons, M. Krbal, J. Tominaga, A. Giussani, K. Perumal, H. Riechert, R. Calarco, T. Uruga. *J. Appl. Phys.* **117**, 125308 (2015).
[35] J. J. Rehr, R. C. Albers. *Rev. Mod. Phys.* **72**, 621 (2000).
[36] M. Krbal, A. V. Kolobov, P. Fons, J. Tominaga, S. R. Elliott, J. Hegedus, T. Uruga. *Phys. Rev. B* **83**, 054203 (2011).
[37] T. Matsunaga, N. Yamada, Y. Kubota. *Acta Crystal. Sec. B* **60**, 685 (2004).
[38] P. Fons, A. V. Kolobov, M. Krbal, J. Tominaga, K. S. Andrikopoulos, S. N. Yannopoulos, G. A. Voyiatzis, T. Uruga. *Phys. Rev. B* **82**, 155209 (2010).
[39] D. Loke, T. H. Lee, W. J. Wang, L. P. Shi, R. Zhao, Y. C. Yeo, T. C. Chong, S. R. Elliott. *Science* **336**, 1566 (2012).
[40] X.-P. Wang, X.-B. Li, N.-K. Chen, Q.-D. Chen, X.-D. Han, S. Zhang, H.-B. Sun. *Acta Mater.* **136**, 242 (2017).
[41] Y. Saito, A. V. Kolobov, P. Fons, K. V. Mitrofanov, K. Makino, J. Tominaga, J. Robertson. *Appl. Phys. Lett. in press* (2019).
[42] A. Koma, K. Yoshimura. *Surf. Sci.* **174**, 556 (1986).